Dynamic Depolarized Light Scattering and Nuclear Magnetic Relaxation Studies of Oligo- and Polystyrenes in Dilute Solutions

Yoshio Takaeda, Takenao Yoshizaki, and Hiromi Yamakawa*

Department of Polymer Chemistry, Kyoto University, Kyoto 606-01, Japan

Received February 28, 1994; Revised Manuscript Received May 4, 1994®

ABSTRACT: The (excess) power spectrum J_Γ of the depolarized component of scattered light was measured for 10 samples of oligo- and polystyrenes, each with the fraction of racemic diads $f_r = 0.59$, in the range of weight-average molecular weight M_w from 3.70×10^2 (trimer) to 1.01×10^4 and also for cumene in cyclohexane at 34.5 °C (Θ) and in carbon tetrachloride at 25.0 °C. The spin–lattice relaxation time T_1 was also determined for the trimer through pentamer and the sample with the highest M_w, and the nuclear Overhauser enhancement NOE, for the trimer and the sample with the highest M_w, both in cyclohexane at 40 °C. It is found that J_Γ may be well represented in terms of a single Lorentzian independently of M_w and solvent and that the relaxation time τ_Γ as defined as the reciprocal of the half-width at half-maximum of J_Γ evaluated at infinite dilution increases with increasing M_w and levels off to an asymptotic value in the limit of $M_w \to \infty$ in each solvent, being consistent with the recent theoretical results on the basis of the helical wormlike (HW) chain model. The reduced relaxation time $k_B T \tau_\Gamma / \eta_0$ with k_B the Boltzmann constant, T the absolute temperature, and η_0 the solvent viscosity is found to be almost independent of solvent for each sample, its asymptotic value in the limit of $M_w \to \infty$ being ca. 4×10^3 Å^3. A comparison is made of the present data for τ_Γ, T_1, and NOE with the HW chain theory, and it is shown that the theory may explain satisfactorily the data in the range of $M_w \gtrsim 10^3$ except for NOE. For $M_w \lesssim 10^3$, the rigid sphere model having the radius equal to the apparent root-mean-square radius of gyration of the HW chain may give a good explanation of all the data. An analysis of the interrelation between these three quantities leads to the simple picture that the nuclear magnetic relaxation is also governed, although approximately, by a single relaxation time identical with τ_Γ.

Introduction

In a series of recent experimental studies of dilute solutions of oligomers and polymers in the unperturbed (Θ) state,[1] our major attention has been given to the elucidation of the relation between the local conformation and stiffness of flexible polymer chains and their equilibrium conformational and steady-state transport properties on the basis of the helical wormlike (HW) chain model.[2,3] In the course of these studies, it has been shown that the conventional scheme of analysis and interpretation of experimental data for high-molecular-weight samples on the basis of the Gaussian chain model may lead to the erroneous conclusion, for instance, that atactic polystyrene (a-PS) chains are stiffer than atactic poly(methyl methacrylate) chains. In the meantime, we have started a reinvestigation of the excluded-volume effects in dilute polymer solutions.[4,5] It has then been found that the two-parameter theory based on the Gaussian chain model is rather a limiting law valid only for extremely large molecular weights M.[5] All the results obtained so far for both unperturbed and perturbed chains indicate that their stiffness and local conformation must be considered in the analysis of their static and steady-state transport properties over a wide range of M in dilute solution. The HW model has proved to be useful for this purpose.

The above fact has raised the hope that the model may provide our deeper understanding of dynamic properties, on the molecular (and atomic) levels, concerning local motions of flexible polymer chains in dilute solution, since they may be considered to be directly related to the local chain conformation. Although a number of experimental investigations have already been made on such dynamic properties of dilute polymer solutions, the results have not been analyzed by the use of a model which can also be applied to static properties. The only exception may probably be our previous analyses of literature data for flexible polymers with sufficiently high M on the basis of the (discrete) HW model.[3,6] Thus, in the present and forthcoming papers, we make experimental studies of dynamic properties of oligomers and polymers in the unperturbed state on the basis of the same model in relation to the static properties studied so far. The dynamic properties we are concerned with are the dynamic depolarized light scattering (LS) and the nuclear magnetic relaxation, both of which may be expressed in terms of the same class of basic time-correlation functions within the framework of the HW theory.[3,7,8] The system studied in the present paper is a-PS in cyclohexane.

As for the power spectrum J_Γ of the depolarized component of light scattered from solutions of flexible polymers,[8] some comments are required here. Very recently, we have shown that the Ono–Okano theory[9] of J_Γ for the Gaussian (spring–bead) model is invalid and presented some new theoretical results on the basis of the HW model.[8] According to our theory, J_Γ may be written in terms of a set of basic time-correlation functions with the "total angular momentum quantum number" $L = 2$ (the tensor mode) and the number of "excited" subbodies $n = 1$ and has no contributions from low-frequency modes corresponding to the Rouse–Zimm modes of the spring–bead model. However, the literature data[10,11] are inconsistent with our theory, and therefore the resolution of this point is one of the purposes of the present study. In general, as M is increased, the ratio of the intensity of the depolarized component to that of the polarized component becomes so small that it is difficult to separate the former from the latter experimentally by the use of an analyzer. As is well-known, the optical anisotropy of a-PS (and also other flexible polymers in general) is very small for $M \gtrsim 5 \times 10^3$ and may be neglected in usual LS measurements. Thus, as pointed out by Bauer et al.[11] themselves, the leak of the polarized component may possibly lead to an incorrect determination of the depolarized-component spectrum. In fact, their observed (total) intensity of the depolarized component increases with increasing M for M

® Abstract published in *Advance ACS Abstracts*, June 15, 1994.

0024-9297/94/2227-4248$04.50/0

Table 1. Values of M_w, x_w, and M_w/M_n for Atactic Oligo- and Polystyrenes

sample	M_w	x_w	M_w/M_n
cumene	1.20×10^2		
OS3[a]	3.70×10^2	3	1.00
OS4	4.74×10^2	4	1.00
OS5	5.78×10^2	5	1.00
OS6	6.80×10^2	5.98	1.00
OS8	9.04×10^2	8.13	1.01
A1000-a[b]	1.23×10^3	11.3	1.03
A2500-a[c]	2.27×10^3	21.2	1.05
A2500-b	3.48×10^3	32.9	1.07
A5000-3	5.38×10^3	51.2	1.03
F1-2	1.01×10^4	96.6	1.03

[a] M_w's of OS3 through OS8 had been determined from GPC.[1] [b] M_w of A1000-a had been determined from LS measurements in cyclohexane at 34.5 °C.[14] [c] M_w's of A2500-a through F1-2 had been determined from LS measurements in MEK at 25.0 °C.[1]

$\lesssim 2 \times 10^6$. This is unphysical from our theoretical point of view above.

In the present work, depolarized LS measurements have also been made on solutions in a good solvent (carbon tetrachloride at 25.0 °C) in order to examine possible effects of the solvent. However, we note that the excluded-volume effect is negligibly small for the present samples, which have weight-average molecular weights $M_w \lesssim 10^4$. The properties we have measured in nuclear magnetic relaxation experiments are the spin–lattice relaxation time T_1 and nuclear Overhauser enhancement NOE, which may be expressed in terms of the same class of basic time-correlation functions as in the case of depolarized spectrum J_Γ, as noted above. We then examine the correlation between the different observables that belong to the same class.

Experimental Section

Materials. All the samples used in this work are the same as those used in the previous studies of the mean-square optical anisotropy,[1] the intrinsic viscosity (in Θ and good solvents),[12-14] the mean-square radius of gyration (in Θ and good solvents),[15,16] the translational diffusion coefficient,[17] and the second virial coefficient A_2.[18,19] They are the fractions separated by preparative gel permeation chromatography (GPC) or fractional precipitation from the standard samples supplied by Tosoh Co., Ltd., and have a fixed stereochemical composition (the fraction of racemic diads $f_r = 0.59$) independent of molecular weight, possessing an n-butyl group at one end of the chain (the initiating end) and a hydrogen atom at the other (the terminating end). The values of M_w, the weight-average degree of polymerization x_w, and the ratio of M_w to the number-average molecular weight M_n are listed in Table 1. As seen from the values of M_w/M_n, all the samples are sufficiently narrow in molecular weight distribution, and, in particular, the samples OS3 through OS5 are completely monodisperse.

Cumene, which corresponds to the monomer of PS, and the solvents cyclohexane, carbon tetrachloride (CCl_4), and methyl ethyl ketone (MEK) were purified according to standard procedures prior to use. We note that although n-hexylbenzene, which had been used in the recent study of A_2 of a-PS,[19] corresponds more strictly to the monomer of the a-PS samples we used, cumene was used as a standard reference as in the previous depolarized light scattering studies.[1,20]

Dynamic Depolarized Light Scattering. The photometer used for all dynamic depolarized LS measurements is the same as that used in the previous studies,[20,21] i.e., a Brookhaven Instruments Model BI-200SM goniometer with a minor modification of its light source part and with a detector alignment newly assembled to incorporate a Fabry–Perot (FP) interferometer in it. It has been described in detail in the previous paper.[20] However, its outline is given below along with a further minor change made for the present study.

Vertically polarized light of wavelength 488 nm from a Spectra-Physics Model 2020 argon ion laser equipped with a Model 583 temperature-stabilized etalon for single-frequency-mode operation was used as a light source. It was made highly vertically (v) polarized by passing through a Gran–Thompson (GT) prism with an extinction ratio smaller than 10^{-5}. The scattered light was measured at a scattering angle of 90°. Its horizontal (H) component, i.e., the depolarized (Hv) component, which was extracted from the total scattered light intensity by the use of the same GT prism as above, was analyzed with a Burleigh Instruments Model RC-110 FP interferometer equipped with a Model RC-670 pair of plane mirrors with a flatness of λ/200 and a reflectivity of 97.5%. The intensity of the Hv component filtered through the FP interferometer was measured by an EMI 9893B/350 photomultiplier (PM) tube. In the present study, we used a pinhole of diameter 25 μm instead of that of diameter 100 μm previously used[20] as a spatial filter, which was placed between the interferometer and the PM tube.

For an accurate determination of the spectrum J_Γ of the depolarized component of scattered light, it is desirable to adopt the method of triple passes, as done previously.[21] Unfortunately, however, in the case of the triple passing, the stability of the (relative) transmittance $T(\omega)$ of the FP interferometer as a function of the angular frequency ω becomes worse with decreasing free spectral range (FSR), i.e., with increasing distance between the mirrors composing the interferometer. Thus all the measurements except for those on cumene were carried out by the normal operation, i.e., the single passing.

As in the previous study,[21] the transmittance $T(\omega)$ was determined by measuring the polarized component of the light scattered from a solution of a PS sample with $M_w = 7.32 \times 10^5$ in MEK at the mass concentration $c \simeq 1 \times 10^{-3}$ g/cm^3 and at 25.0 or 34.5 °C, following Ouano and Pecora.[22]

The width of the spectrum J_Γ becomes narrower as M_w is increased, since the relaxation of the orientation of the repeat unit becomes slower. Thus, the FSR of the interferometer (i.e., the distance between the mirrors) was changed from 4.7×10^{10} to 7.0×10^{12} rad/s, depending on this width, in order to attain an appropriate resolution.

The value of FSR (δ) for each setting was determined by the use of the sodium doublet of separation 0.597 nm at 589.3 nm for FSR $\gtrsim 5 \times 10^{12}$ rad/s, of the ^{4}He hyperfine structure interval of 1.0 cm^{-1} at 587.5 nm associated with the 2^3P–3^3D transition[23] for $4 \times 10^{11} \lesssim$ FSR $\lesssim 2 \times 10^{12}$ rad/s, and of the Brillouin shift $\Delta\omega_B$ of 3.53×10^{10} rad/s in the Rayleigh–Brillouin spectrum of pure benzene at 25.0 °C at 1 atm for $10^{11} \lesssim$ FSR $\lesssim 3 \times 10^{11}$ rad/s. For FSR $\lesssim 10^{11}$ rad/s, the distance between the mirrors was directly measured. We note that the value of $\Delta\omega_B$ was calculated from the relation[24]

$$\Delta\omega_B = c_s k \tag{1}$$

with c_s the (adiabatic) speed of sound and k the magnitude of the scattering vector, using the value 1.29×10^3 m/s of c_s for benzene under the same condition. For the present measurements in which the scattering angle is fixed at a right angle, k may be set equal to $2\sqrt{2}\pi/\tilde{\lambda}$ with $\tilde{\lambda}$ the wavelength of the incident light in the medium. In Figure 1 are shown a spectrum of the sodium doublet (a) and that of the hyperfine structure of ^{4}He at 587.5 nm (b) as examples. We note that these spectra were measured with a narrow band-pass filter of central wavelength 588.3 nm and full width at half-maximum 3.4 nm, which is different from the one used for the determination of J_Γ. We also note that the (relative) intensities themselves of the two peaks in the respective spectra are not absolute since they were biased by the filter. Figure 2 shows an example of the Rayleigh–Brillouin spectrum of pure benzene.

Measurements were carried out on solutions in cyclohexane at 34.5 °C (Θ) and in CCl_4 at 25.0 °C. The most concentrated solutions of each sample were prepared gravimetrically and made homogeneous by continuous stirring at ca. 50 °C for 1–3 days in cyclohexane and for 1 day in CCl_4. These solutions and solvents were optically purified by filtration through a Teflon membrane of pore size 0.1 or 0.45 μm. The solutions of lower concentrations were obtained by successive dilution. The weight concentrations

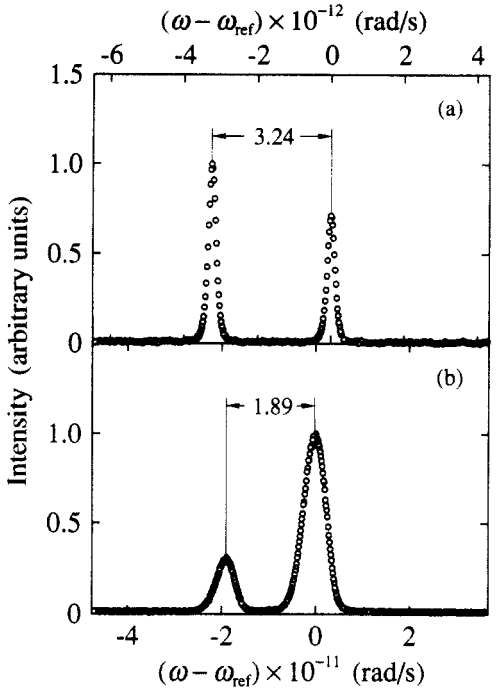

Figure 1. Spectra of the sodium doublet (a) and the hyperfine structure of ^{4}He at 587.5 nm (b) as functions of the deviation $\omega-\omega_{ref}$ of the angular frequency ω from the (reference) frequency ω_{ref} for the peak with larger ω.

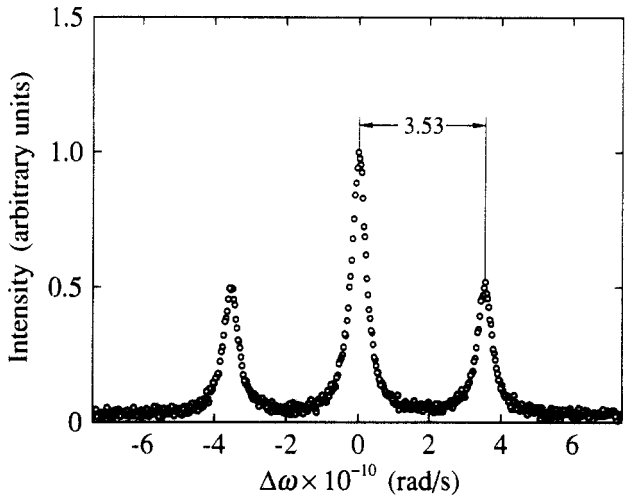

Figure 2. Rayleigh–Brillouin spectrum as a function of the difference $\Delta\omega$ between the angular frequencies of the scattered and incident light waves for pure benzene at 25.0 °C at 1 atm.

of the test solutions were converted to the solute mass concentrations c (in g/cm^3) by the use of the densities of the solutions.

Before and after each measurement on the solution or solvent, the transmittance of the FP interferometer was determined in the manner as described above. (We note that the Hv component scattered from pure benzene was not measured since the absolute intensity of the spectrum was not necessary.) In the present measurements, the finesse could be kept at 60–65 for the triple passing and at 45–50 for the single passing during a single measurement, which took ca. 40 min for both cases.

Nuclear Magnetic Relaxation. T_1 of ^{13}C was determined for aliphatic carbon atoms of the samples OS3, OS4, OS5, and F1-2 by the inversion–recovery method with a pulse sequence $\pi-t-\pi/2$ on a JEOL JNM GX-400 spectrometer at 100.4 MHz. NOE for each of those carbon atoms of the samples OS3 and F1-2 was evaluated from the ratio of the integrated intensity of its peak obtained with complete noise decoupling of protons to that obtained with gated decoupling only during data acquisition. A pulse delay was taken to be longer than 5 times as long as the largest T_1 of aliphatic carbon atoms under observation. Measurements were carried out on solutions in cyclohexane at 40 °C with a lock signal obtained from an external C_6D_{12} tube. The measurement temperature is somewhat higher than the Θ temperature 34.5 °C. (The reason for this is that it was difficult to keep using liquid nitrogen as refrigerant for overnight measurements in our common facility.) The solutions were not degassed since T_1's of interest rarely exceed 1 s, as shown later.

Results

Depolarized Spectrum J_T and Relaxation Time τ_T. As shown in the previous paper,[21] if the FSR is chosen to be sufficiently larger than the width of the (true) spectrum $I(\Delta\omega)$ as a function of the difference $\Delta\omega$ between the angular frequencies of the scattered and incident light waves, then the observed (apparent) spectrum $I_{ap}(\Delta\omega_{ap})$ as a function of the difference $\Delta\omega_{ap}$ between those for the peak of the transmittance of the FP interferometer and of the incident light may be written in the form

$$I_{ap}(\Delta\omega_{ap}) = \int_{-\delta/2}^{\delta/2} T(\Delta\omega-\Delta\omega_{ap})\, I(\Delta\omega)\, d(\Delta\omega) \qquad (2)$$

where δ is the value of the FSR determined experimentally as mentioned in the Experimental Section and $T(\Delta\omega)$ is the transmittance of the FP interferometer as a function of the deviation $\Delta\omega$ of the angular frequency from that for the peak. $T(\Delta\omega)$ may be determined experimentally as mentioned in the Experimental Section and may be well fitted by the equation

$$T(\Delta\omega) = C[1 + (2F/\delta)^2(\Delta\omega)^2]^{-3} \qquad (3)$$

in the case of the triple passing and by the equation

$$T(\Delta\omega) = C[1 + (2F/\delta)^2(\Delta\omega)^2]^{-1} \qquad (4)$$

in the case of the single passing, where C is a factor representing the maximum transmittance in each case and F is a parameter representing the resolution of the FP interferometer. (Note that F is equal to the finesse in the case of the single passing.) Thus $I(\Delta\omega)$ may be determined by solving the integral equation (2) numerically as follows.

We first determine the values of the parameters C and F in eq 3 or eq 4 so that the squared difference between the observed transmittance T and the one calculated from eq 3 or eq 4 may be minimized. Then, we express $I(\Delta\omega)$ as a sum of a constant term and several normalized Lorentzians, i.e.

$$I(\Delta\omega) = A_0 + \sum_{i=1}^{m} (A_i c_i/\pi)[1 + (c_i\Delta\omega)^2]^{-1} \qquad (5)$$

and determine the coefficients $(A_0, A_1, ..., A_m) = \{A_{m+1}\}$ and $(c_1, c_2, ..., c_m) = \{c_m\}$ so that the sum f of residual errors defined by

$$f(\{A_{m+1}\},\{c_m\}) = \sum_{i=1}^{N} |I_{ap,i} - I_{ap}(\Delta\omega_i)|^2 \qquad (6)$$

may be minimized, where $I_{ap,i}$ is the (apparent) intensity observed at $\Delta\omega_{ap} = \Delta\omega_i$ and $I_{ap}(\Delta\omega_i)$ is the (apparent) intensity calculated from eq 2 with eq 3 or eq 4 (with proper values of the parameters) and with eq 5.

In general, the spectrum $I_{Hv}(\Delta\omega)$ of the depolarized component of scattered light determined from the apparent spectrum $I_{Hv,ap}(\Delta\omega)$ as above has contributions not only from solute molecules but also from solvent molecules. Fortunately, however, the optical anisotropy of the solvents, cyclohexane and CCl_4, used in the present study is negligibly small compared to that of the solute a-PS. Quantitatively, for a solution of cumene in CCl_4 at $c \simeq 0.18$ g/cm^3, the solvent contribution amounts at most only to ca. 2% of the total intensity, as shown in Figure 2 of ref 20. This is also the case with the solvent cyclohexane,

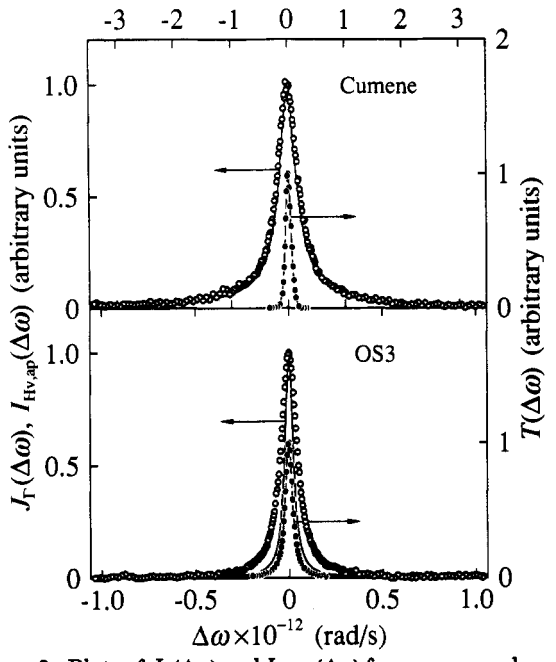

Figure 3. Plots of $J_\Gamma(\Delta\omega)$ and $I_{Hv,ap}(\Delta\omega)$ for cumene and sample OS3 in cyclohexane at 34.5 °C at c = 0.109 and 0.112 g/cm^3, respectively, and also $T(\Delta\omega)$ against $\Delta\omega$. The solid curve and unfilled circles represent the values of J_Γ and $I_{Hv,ap}$, respectively, and the filled circles and dashed curve represent the observed and best-fit values of T, respectively.

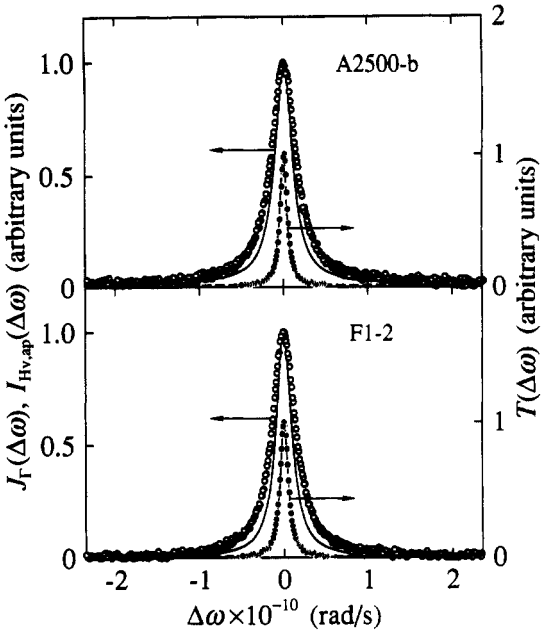

Figure 4. Plots of $J_\Gamma(\Delta\omega)$ and $I_{Hv,ap}(\Delta\omega)$ for samples A2500-b and F1-2 in cyclohexane at 34.5 °C at c = 0.110 and 0.098 g/cm^3, respectively, and also $T(\Delta\omega)$ against $\Delta\omega$. See caption for Figure 3.

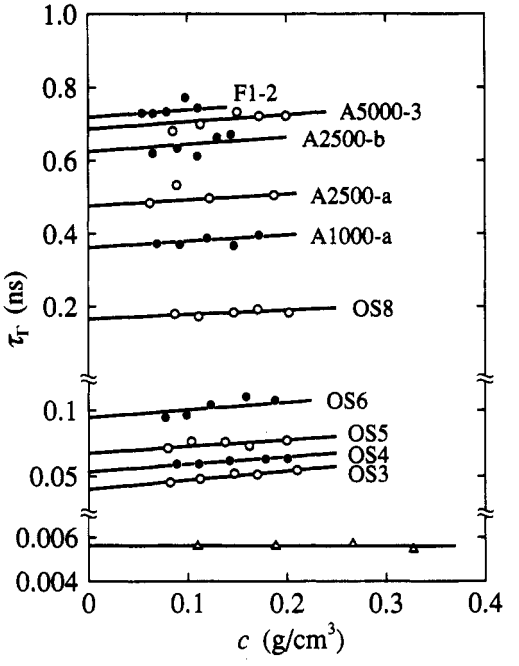

Figure 5. Plots of τ_Γ against c for all a-PS samples in cyclohexane at 34.5 °C. The triangles represent the values for cumene.

although we do not show the results explicitly. As M_w is increased, the optical anisotropy of the solute a-PS becomes large and its spectrum $I_{Hv}(\Delta\omega)$ becomes extremely narrow compared to that of the solvent ($M_w \lesssim 10^4$), so that the solvent contribution to the whole spectrum becomes less and less important. Therefore, we do not take account of that contribution and regard $I_{Hv}(\Delta\omega)$ thus obtained as the intrinsic depolarized spectrum $J_\Gamma(\Delta\omega)$ due to the solute a-PS, and the individual Lorentzians obtained from the above procedure may be regarded as being associated with the actual modes of molecular motions.

In practice, we solve eq 2 with six Lorentzians, i.e., put m = 6 in eq 5. Figure 3 shows plots of J_Γ and also $I_{Hv,ap}(\Delta\omega)$ thus obtained for solutions of cumene and OS3 in cyclohexane at 34.5 °C at c = 0.109 and 0.112 g/cm^3, respectively, against $\Delta\omega$ along with $T(\Delta\omega)$ determined before the respective measurements. Figure 4 shows similar plots for solutions of A2500-b and F1-2 in cyclohexane at 34.5 °C at c = 0.110 and 0.098 g/cm^3, respectively. It is interesting to note that, for all cases including those shown in Figures 3 and 4, the coefficients c_i of the six Lorentzians have been found to be the same, indicating that $J_\Gamma(\Delta\omega)$ may be fitted by a single Lorenztian. This is consistent with our theory,[8] although it predicts that there is a minor contribution of another Lorentzian.

Then, we consider the (apparent) relaxation time τ_Γ as defined as the reciprocal of the half-width at half-maximum (hwhm), which is just the hwhm of the single Lorentzian in the present case. Figures 5 and 6 show plots of τ_Γ against c for all a-PS samples in cyclohexane at 34.5 °C and in CCl_4 at 25.0 °C, respectively. All the plots follow the straight lines, and the respective values of τ_Γ at infinite dilution may be evaluated from the intercepts. It is seen that, in both solvents, τ_Γ increases with increasing c for all the samples except for cumene and that this dependence is larger in CCl_4 than in cyclohexane for $M_w \gtrsim 10^3$.

The values of τ_Γ thus obtained at infinite dilution are given in Table 2 along with those of $k_BT\tau_\Gamma/\eta_0$ with k_B the Boltzmann constant, T the absolute temperature, and η_0 the solvent viscosity. The latter values have been calculated from the former with the values 0.768 and 0.904 cP of η_0 for cyclohexane at 34.5 °C and CCl_4 at 25.0 °C, respectively. The quantity $k_BT\tau_\Gamma/\eta_0$ must be independent of the solvent condition if the motion of the small molecule or the motional unit in the polymer chain may be described in the diffusion limit and if the local chain conformation does not depend on that condition. Since the values of $k_BT\tau_\Gamma/\eta_0$ for cumene in the two solvents agree well with each other, the dynamics that governs τ_Γ may be considered to be described in this limit as far as these two solvents are concerned. Although the values of $k_BT\tau_\Gamma/\eta_0$ in cyclohexane are somewhat smaller than those in CCl_4 for $M_w \gtrsim 2\times10^3$, we may conclude that there is no appreciable difference between them in the two solvents at infinite dilution.

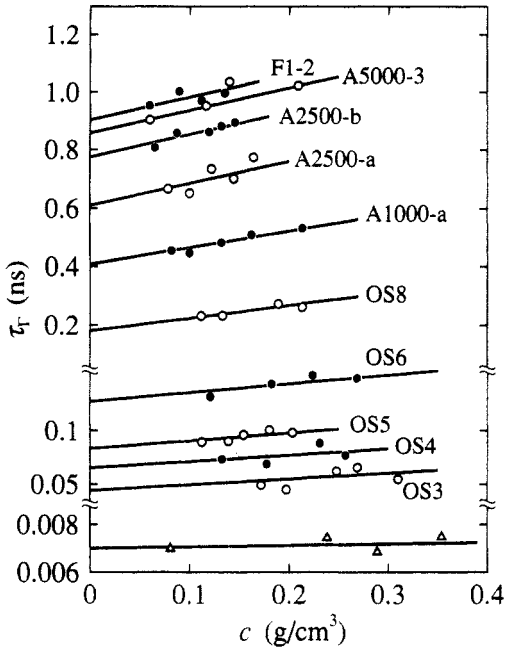

Figure 6. Plots of τ_T against c for all a-PS samples in CCl_4 at 25.0 °C. The triangles represent the values for cumene.

Table 2. Values of τ_T and $k_BT\tau_T/\eta_0$ for Atactic Oligo- and Polystyrenes in Cyclohexane at 34.5 °C and in Carbon Tetrachloride at 25.0 °C

	cyclohexane (34.5 °C)		carbon tetrachloride (25.0 °C)	
sample	τ_T, ns	$k_BT\tau_T/\eta_0$, Å^3	τ_T, ns	$k_BT\tau_T/\eta_0$, Å^3
cumene	0.0056_2	$3.1_1 \times 10$	0.0070_0	$3.1_9 \times 10$
OS3	0.040_0	$2.2_1 \times 10^2$	0.044_3	$2.0_2 \times 10^2$
OS4	0.053_5	$2.9_6 \times 10^2$	0.065_2	$2.9_7 \times 10^2$
OS5	0.067_6	$3.7_4 \times 10^2$	0.083_5	$3.8_0 \times 10^2$
OS6	0.094_5	$5.2_3 \times 10^2$	0.12_7	$5.7_8 \times 10^2$
OS8	0.16_6	$9.1_8 \times 10^2$	0.18_0	$8.1_9 \times 10^2$
A1000-a	0.36_3	$2.0_1 \times 10^3$	0.40_7	$1.8_5 \times 10^3$
A2500-a	0.47_7	$2.6_4 \times 10^3$	0.61_0	$2.7_8 \times 10^3$
A2500-b	0.62_5	$3.4_5 \times 10^3$	0.77_4	$3.5_2 \times 10^3$
A5000-3	0.68_7	$3.8_0 \times 10^3$	0.85_8	$3.9_1 \times 10^3$
F1-2	0.71_9	$3.9_8 \times 10^3$	0.90_3	$4.1_1 \times 10^3$

Figure 7 shows plots of $k_BT\tau_T/\eta_0$ at infinite dilution against the logarithm of M_w for a-PS. The unfilled and filled circles represent the present values in cyclohexane at 34.5 °C and in CCl_4 at 25.0 °C, respectively. The solid curve connects smoothly the data points for OS3 through F1-2, and the dashed line segment connects those for cumene and OS3. The unfilled triangles represent the data obtained by Bauer et al.[11] in CCl_4 at 22 °C, and the filled triangles represent those obtained by Strehle et al.[25] in bicyclohexyl at 21.0–86.0 °C, both of which were determined at finite concentrations. Although Bauer et al. made measurements also on samples with $M_w \gtrsim 10^4$, the spectra for them were decomposed into two Lorentzians corresponding to slow and fast modes.[11] Thus we have omitted those data. The present data points seem to level off to an asymptotic value ca. 4×10^3 Å^3 in the limit of $M_w \to \infty$, being consistent with our theory.[8] In contrast to this, the data points by Bauer et al. and Strehle et al. seem to increase without limit with increasing M_w. As for the data by Bauer et al., it is plausible to consider that this is due to the residual contribution of the polarized component, which makes the spectrum sharp, since they themselves pointed out the possibility of the leak of that component, as mentioned in the Introduction. At any rate, it is unphysical that τ_T increases with increasing M_w even in the range of M_w where the unperturbed dimension of a given polymer chain may be described by the Gaussian

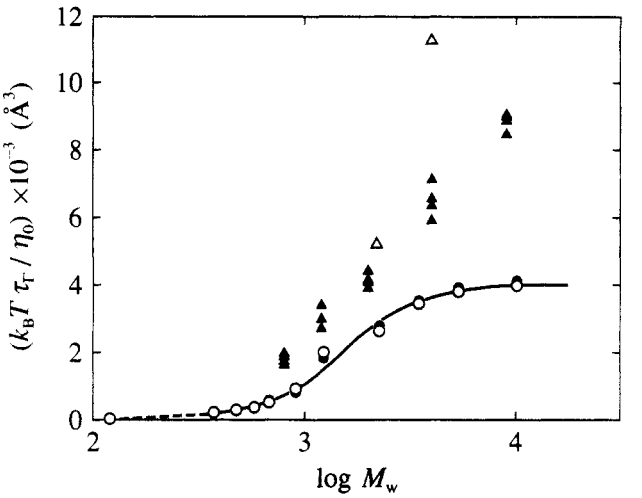

Figure 7. Plots of $k_BT\tau_T/\eta_0$ at infinite dilution against the logarithm of M_w for a-PS: (○) in cyclohexane at 34.5 °C; (●) in CCl_4 at 25.0 °C; (△) in CCl_4 at 22 °C by Bauer et al.;[11] (▲) in bicyclohexyl at 21.0–86.0 °C by Strehle et al.[25]

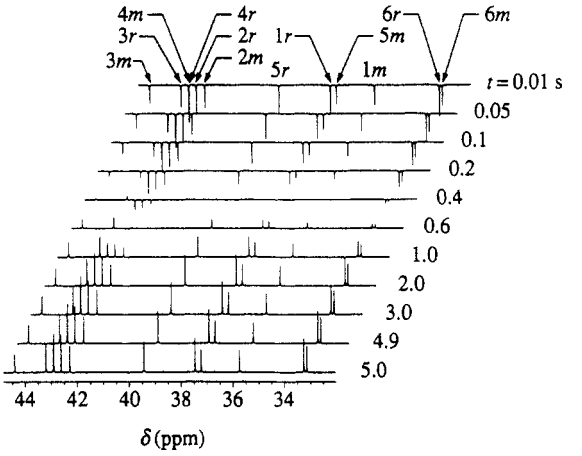

Figure 8. ^{13}C NMR spectra of aliphatic carbon atoms of sample OS3 in cyclohexane at 40 °C at c = 0.180 g/cm^3. The labels $x\alpha$ (x = 1–6; α = m, r) indicate the assignments of the respective peaks, where x is the carbon number as defined in the caption of Table 3 and α indicates whether the diad in the sample is meso (m) or racemic (r).

chain model. Therefore, we do not inquire into the sources of the difference between the present and literature data and also of that between the literature data of the two groups.

Spin–Lattice Relaxation Time T_1 and Nuclear Overhauser Enhancement NOE. As a typical example, Figure 8 shows ^{13}C NMR spectra obtained by the inversion-recovery method for the sample OS3 in cyclohexane at 40 °C at c = 0.180 g/cm^3 in the range of the chemical shift δ from 32 to 45 ppm, in which there are the peaks associated with the aliphatic carbon atoms except for those in the initiating-end (n-butyl) group. We have identified each peak of the spectra by the use of the assignments obtained by Ray et al.[26] and labeled it with the index $x\alpha$ (x = 1–6; α = m, r), where x is the carbon atom number and α indicates whether the diad in the sample is meso (m) or racemic (r). The carbon atoms have been numbered from the methylene carbon atom adjacent to the initiating-end (n-butyl) group to the terminating-end methylene carbon atom, as explicitly shown in the caption of Table 3. Note that the oligomer samples are mixtures of stereoisomers. Then T_1 of ^{13}C for each carbon atom has been evaluated by the standard procedure offered by JEOL Co., Ltd. (For an examination of this procedure, we have compared the values of T_1 obtained by this procedure for several peaks

Table 3. Values of $T_{1,\alpha}$ and NOE_α ($\alpha = m, r$) for OS3 in Cyclohexane at 40 °C

$C_4H_9CH_2CH(C_6H_5)CH_2CH(C_6H_5)CH_2CH_2(C_6H_5)$

carbon atom no.	($T_{1,m}$, $T_{1,r}$), s		(NOE_m, NOE_r):
	c = 0.092 g/cm³	c = 0.180 g/cm³	c = 0.093 g/cm³
1	(0.77, 0.79)	(0.56, 0.67)	(3.0, 2.9)
2	(1.13, 1.00)	(0.93, 0.99)	(2.7, 2.7)
3	(0.61, 0.53)	(0.44, 0.52)	(2.9, 2.9)
4	(0.97, 1.14)	(0.89, 0.89)	(3.0, 3.0)
5	(0.65, 0.79)	(0.59, 0.62)	(2.9, 2.9)
6	(0.84, 0.94)	(0.79, 0.80)	(3.0, 2.9)

Table 4. Values of $T_{1,\alpha\beta}$ ($\alpha, \beta = m, r$) for OS4 in Cyclohexane at 40 °C

$C_4H_9CH_2CH(C_6H_5)CH_2CH(C_6H_5)CH_2CH(C_6H_5)CH_2CH_2(C_6H_5)$

carbon atom no.	($T_{1,mm}$, $T_{1,mr}$, $T_{1,rm}$, $T_{1,rr}$), s	
	c = 0.084 g/cm³	c = 0.165 g/cm³
1	(0.50, –, 0.58, 0.60)	(0.46, –, 0.51, 0.53)
2	(–, 0.75, 0.72, 0.74)	(–, 0.67, 0.62, 0.71)
3	(0.37, –, 0.40, 0.44)	(0.32, –, 0.34, 0.34)
4	(0.67, 0.65, 0.67, 0.74)	(0.58, 0.59, 0.59, 0.64)
5	(0.39, 0.37, 0.38, 0.40)	(0.34, 0.33, 0.34, 0.34)
6	(0.75, 0.75, 0.75, 0.79)	(0.64, 0.68, 0.68, 0.72)
7	(0.48, –, 0.54, 0.59)	(0.44, –, 0.48, 0.48)
8	(0.60, 0.70, 0.68, 0.65)	(0.57, 0.56, 0.63, 0.62)

with those evaluated by ourselves.) The values of T_1 thus obtained are given in Table 3 along with those of NOE for the respective carbon atoms. Although we could not estimate the experimental error in the raw data, the error in the evaluation of T_1 from the spectra is at most ca. ±2%. It is seen that the values of NOE obtained for the sample OS3 are ca. 3 for all carbon atoms, corresponding to the one in the narrowing limit.

In Tables 4–6 are given the values of T_1 determined similarly for the samples OS4, OS5, and F1-2, respectively. Those of NOE for the sample F1-2 are also given in Table 6. For the identification of the peaks of their spectra, we have used the assignments obtained in the previous ^{13}C NMR study of the samples OS4 and OS5[27] and those obtained by Sato et al.[28] for PS samples with sufficiently large M_w. For the sample OS5, the individual assignments for the 4th, 6th, and 10th carbon atoms and also the distinction between the peaks for the first two could not be made,[27] so that only their mean values of T_1 are given in Table 5. For the sample F1-2, we have only been able to determine those mean values associated with the intermediate carbon atoms, as given in Table 6. Although it has been considered so far for flexible vinyl polymers that the ratio of values of T_1 of methine to methylene carbon atoms is just equal to 2, the ratio 1.7 evaluated from the present results for the sample F1-2 is somewhat smaller than 2, in accordance with the experimental result recently obtained by Radiotis et al.[29] for poly(vinyl chloride). As suggested by them, the decrease in the ratio seems to imply that the orientational relaxation of the C–H internuclear vectors in the methylene group is faster than that in the methine group.

Now, for the oligomer samples, it is seen from Tables 3–5 that T_1 and also NOE for a given carbon atom depend somewhat on the stereoregularity, as is natural. However, since we are interested in their dependences on M_w, we ignore the difference between their values for the stereoisomers and simply consider only the mean values for the initiating-end methine (second) carbon atom (i), terminating-end methylene (last) one (t), and the center (or intermediate) methine ones (c). Figure 9 shows plots of the reciprocal of the mean $n_{CH}T_1$ against c for these carbon atoms of the samples OS3, OS4, OS5, and F1-2, where n_{CH} is the number of C–H bonds associated with the carbon atom under consideration. The mean values for the center methine carbon atoms of OS4 and OS5 are the averages over the 4th and 6th atoms. The unfilled circles and the unfilled and filled triangles represent the data for the center methine carbon atom and the initiating-end methine and terminating-end methylene ones, respectively. Extrapolation is made to infinite dilution from a pair of data at two concentrations for each carbon atom, following the straight line indicated. The values of $n_{CH}T_1$ thus evaluated at infinite dilution are summarized in Table 7. It is seen that the values of $n_{CH}T_1$ for the terminating-end methylene carbon atoms are appreciably larger than the others. Note that, for flexible polymer chains, $n_{CH}T_1$ in general increases with decreasing relaxation time of the orientation of the C–H internuclear vector.

Figure 10 shows plots of $n_{CH}T_1$ at infinite dilution against the logarithm of M_w. The unfilled circles and the unfilled and filled triangles represent the values for the center methine carbon atom and the initiating-end methine and terminating-end methylene ones, respectively, and the solid curves connect smoothly the data points for the respective atoms. The vertical line segments attached to the data points indicate the limit of experimental error, which is due to the ambiguity in the evaluation of T_1 mentioned above. The curve for the center carbon atom has been drawn by considering the results obtained by Matsuo et al.[30] for poly(fluorostyrene) from ^{19}F NMR, which show that T_1 decreases with increasing M_w and reaches its $M_w \to \infty$ asymptotic value at $M_w \simeq 10^4$. This is consistent with the present results for τ_Γ given in the last subsection.

Discussion

HW Theory. In order to make a comparison of the present results of depolarized LS and nuclear magnetic relaxation measurements with the HW theory in the subsections that follow, it is convenient to here briefly summarize the theoretical results for J_Γ, T_1, and NOE.

For the single (discrete) HW chain composed of N identical rigid subbodies, the power spectrum $J_\Gamma(\Delta\omega)$ of the depolarized component of the light scattered from it may be written in the form[8]

$$J_\Gamma(\Delta\omega) = \sum_{k=\text{odd}} \sum_{j=-2}^{2} A_k^j \frac{\tau_{2,k}^j}{1 + (\Delta\omega\tau_{2,k}^j)^2} \tag{7}$$

where

$$\tau_{2,k}^j = 1/\lambda_{2,k}^j \tag{8}$$

$$A_k^j = \frac{12\pi}{(N+1)} B_k^j \cot^2\left[\frac{\pi k}{2(N+1)}\right] \tag{9}$$

with

$$B_k^j = (8\pi^2)^{-1} \left|\sum_{j'=-2}^{2} \alpha_2^{j'} R_{2,k}^{ij'}\right|^2 \tag{10}$$

In eq 8, $\lambda_{2,k}^j$ are the eigenvalues of the matrix representation of the diffusion operator associated with the subspace spanned by the basis set with the total angular momentum quantum number $L = 2$ and the number of excited subbodies $n = 1$. Precisely, $J_\Gamma(\Delta\omega)$ is the Fourier–Laplace transform of a linear combination of the basic time-correlation functions associated with that subspace. We use the augmented eigenvalues $\lambda_{2,k}^j$ given by eq 25 of

Table 5. Values of $T_{1,\alpha\beta\gamma}$ ($\alpha, \beta, \gamma = m, r$) for OS5 in Cyclohexane at 40 °C

1 2 3 4 5 6 7 8 9 10
$C_4H_9CH_2CH(C_6H_5)CH_2CH(C_6H_5)CH_2CH(C_6H_5)CH_2CH(C_6H_5)CH_2CH_2(C_6H_5)$

carbon atom no.	($T_{1,mmm}$, $T_{1,mmr}$, $T_{1,mrm}$, $T_{1,mrr}$, $T_{1,rmm}$, $T_{1,rmr}$, $T_{1,rrm}$, $T_{1,rrr}$), s	
	c = 0.085 g/cm³	c = 0.179 g/cm³
1	(0.36, 0.41, –, 0.50, –, –, 0.46, –)	(0.47, 0.42, –, 0.38, –, –, 0.35, –)
2	(–, –, –, –, –, –, 0.59, –)	(–, –, –, –, –, –, 0.45, –)
3	(–, –, 0.26, 0.33, –, –, 0.31, –)	(–, –, 0.25, 0.25, –, –, 0.22, –)
4	0.53	0.42
5	(–, 0.28, 0.26, –, 0.33, 0.27, –, 0.31)	(–, 0.19, –, –, 0.25, 0.22, –, 0.25)
6	0.53	0.42
7	(–, –, 0.30, 0.31, –, –, 0.25, –)	(–, –, 0.22, 0.24, –, –, 0.24, –)
9	(–, 0.50, –, 0.44, 0.46, 0.49, 0.46, 0.43)	(–, 0.34, –, 0.41, 0.37, 0.40, 0.35, 0.34)
10	0.60	0.49

Table 6. Values of T_1 and NOE for F1-2 in Cyclohexane at 40 °C

carbon atom	T_1, s		NOE:
	c = 0.089 g/cm³	c = 0.111 g/cm³	c = 0.097 g/cm³
methine	0.25	0.25	1.6
methylene	0.15	0.15	1.7

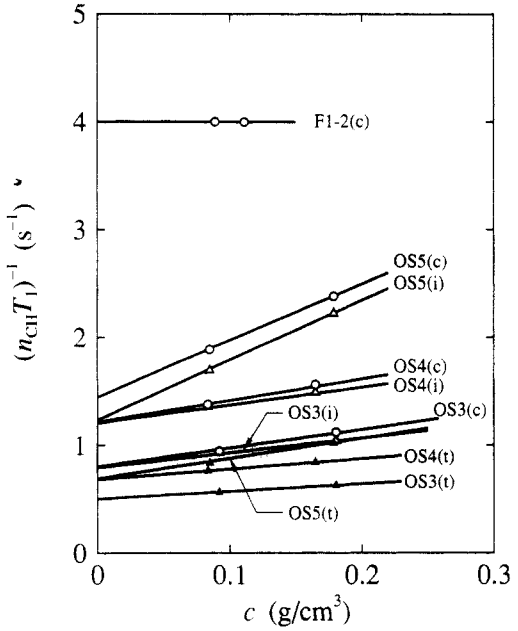

Figure 9. Plots of $(n_{CH}T_1)^{-1}$ of ^{13}C against c for samples OS3, OS4, OS5, and F1-2 in cyclohexane at 40 °C: (○) center methine carbon atoms (c); (△) initiating-end methine carbon atoms (i); (▲) terminating-end methylene carbon atoms (t).

Table 7. Values of $n_{CH}T_1$ for Initiating-End (i) and Center (c) Methine and Terminating-End (t) Methylene Carbon Atoms of Atactic Oligo- and Polystyrenes in Cyclohexane at 40 °C at Infinite Dilution

carbon atom	$n_{CH}T_1$, s	carbon atom	$n_{CH}T_1$, s
OS3(c)	1.25	OS4(t)	1.47
OS3(i)	1.26	OS5(c)	0.69
OS3(t)	2.00	OS5(i)	0.81
OS4(c)	0.82	OS5(t)	1.45
OS4(i)	0.82	F1-2(c)	0.25

ref 6 (or eq 49 of ref 8) which takes partly into account the interactions with the complementary subspace. Thus $\lambda^j_{2,k}$ may readily be calculated for given values of N and the six model parameters. They are the constant differential-geometrical curvature κ_0 and torsion τ_0 of the characteristic helix, the static stiffness parameter λ^{-1}, the bond length a, and the translational and rotatory friction coefficients ζ_t and ζ_r of the subbody. In eq 10, α^j_2 is the spherical tensor component of the polarizability tensor affixed to the subbody and $R^{ij'}_{2,k}$ is the transformation

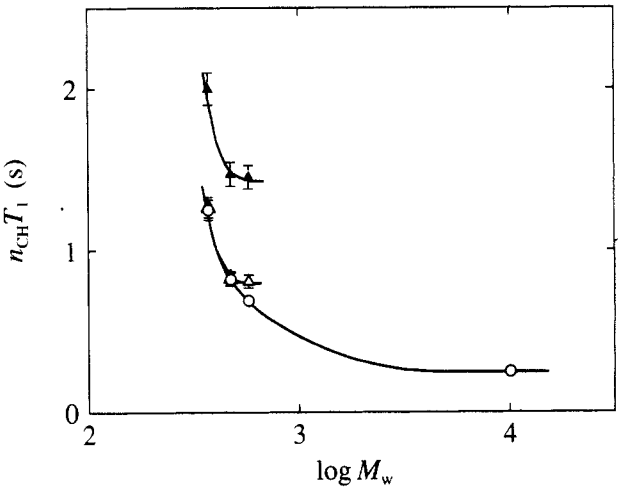

Figure 10. Plots of $n_{CH}T_1$ of ^{13}C at infinite dilution against the logarithm of M_w for a-PS in cyclohexane at 40 °C: (○) center methine carbon atoms; (△) initiating-end methine carbon atoms; (▲) terminating-end methylene carbon atoms.

matrix associated with the eigenvalue problem of the matrix mentioned above and is given by eq 40 of ref 8. We note that $R^{ij'}_{2,k}$ depends on the parameters κ_0, τ_0, and λ^{-1}.

We assume that the nuclear magnetic spin relaxes due to the heteronuclear dipolar interaction between two unlike spins I and S, with spin I observed and spin S irradiated and with the internuclear distance r. Then T_1 and NOE for the HW chain introduced above may be given by[31]

$$T_1^{-1} = (1/20)K^2r^{-6}[J_0(\omega_S - \omega_I) + 3J_1(\omega_I) + 6J_2(\omega_S + \omega_I)] \quad (11)$$

$$\mathrm{NOE} = 1 + \frac{\gamma_S}{\gamma_I}\left[\frac{6J_2(\omega_S + \omega_I) - J_0(\omega_S - \omega_I)}{J_0(\omega_S - \omega_I) + 3J_1(\omega_I) + 6J_2(\omega_S + \omega_I)}\right] \quad (12)$$

where

$$K = \hbar\gamma_I\gamma_S \quad (13)$$

$$J_m(\omega) = 2\sum_{k=1}^{N}(Q^0_{pk})^2\sum_{j=-2}^{2}\frac{A^j_{2,k}\tau^j_{2,k}}{1 + (\omega\tau^j_{2,k})^2} \quad (14)$$

with

$$Q^0_{pk} = [2/(N+1)]^{1/2}\sin[\pi pk/(N+1)] \quad (15)$$

and with $\tau^j_{2,k}$ and $A^j_{2,k}$ being given by eqs 8 and 26 of ref 31, respectively. In the above expressions, $\hbar$ is Dirac's constant (Planck's constant divided by 2π), γ_I and γ_S are the gyromagnetic ratios of spins I and S, respectively, and ω_I and ω_S are their Larmor angular frequencies. Note

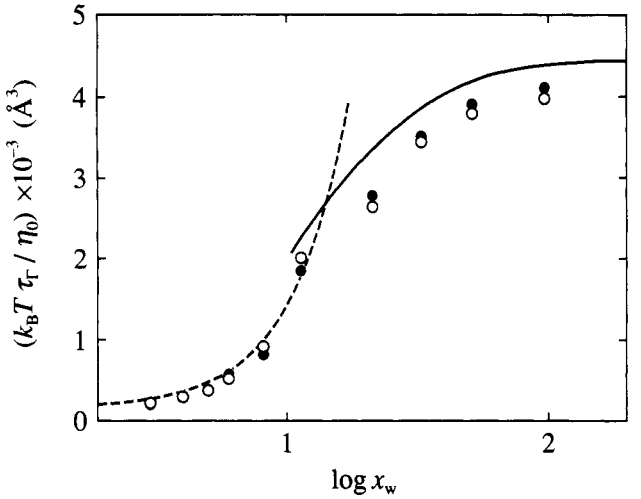

Figure 11. Plots of $k_BT\tau_\Gamma/\eta_0$ against the logarithm of x_w for a-PS: (○) in cyclohexane at 34.5 °C; (●) in CCl_4 at 25.0 °C. The solid and dashed curves represent the theoretical values for the HW model and the effective rigid sphere model, respectively.

that I and S are ^{13}C and ^1H, respectively, in the present case, so that $I = S = 1/2$. In eq 14, the index p indicates the subbody number.

It is interesting to note that J_Γ, T_1, and NOE may be expressed in terms of completely the same class of $\tau^j_{2,k}$ or $\lambda^j_{2,k}$. The so-called Rouse–Zimm relaxation times are not included in this class, so that none of $\tau^j_{2,k}$ diverges with increasing N (or M). Therefore, our theory predicts that both τ_Γ and T_1 approach the respective finite asymptotic values in the limit of $M \to \infty$.

Dependence of τ_Γ on x_w. Now we proceed to make a comparison of the present data for τ_Γ with the HW theory. Figure 11 shows plots of $k_BT\tau_\Gamma/\eta_0$ against the logarithm of x_w for a-PS in cyclohexane at 34.5 °C (unfilled circles) and in CCl_4 at 25.0 °C (filled circles). The solid curve represents the HW theoretical values for τ_Γ as the reciprocal of the hwhm of J_Γ calculated from eqs 7–10 with the values of the (static) model parameters,[5] i.e., $\lambda^{-1}\kappa_0 = 3.0$, $\lambda^{-1}\tau_0 = 6.0$, $\lambda^{-1} = 20.6$ Å, and $\lambda a = 0.14$ ($a = 2.88$ Å), those of the (dynamic) parameters, i.e., $r_1 \equiv \zeta_t/3\pi\eta_0 a = 1.0$ and $r_2 \equiv \zeta_t/a^2\zeta_r = 8.0$, and those of the Cartesian components of the polarizability tensor α of the subbody given by[1,8]

$$\alpha = \begin{pmatrix} 2.10 & 0.28 & 0 \\ 0.28 & 2.13 & 0 \\ 0 & 0 & -1.70 \end{pmatrix} \text{Å}^3 \quad \text{(a-PS)} \qquad (16)$$

which is expressed in the localized coordinate system affixed to the subbody and is independent of the subbody number p. We note that the above value of λa has been evaluated from eq 22 of ref 32 with the value 0.141 of $\lambda\Delta s = \lambda M_0/M_L$, where M_0 is the molecular weight of the repeat unit and is taken to be 104 for a-PS, and M_L is the shift factor as defined as the molecular weight per unit contour length and has been determined to be 35.8 Å^{-1} for a-PS.[5] We also note that the number N of subbodies in the chain has been set equal to x_w.

The above calculation of the theoretical values requires some remarks. Among the above parameters, only r_2 has been treated as an adjustable one, and then the theoretical asymptotic value of $k_BT\tau_\Gamma/\eta_0$ in the limit of $x_w \to \infty$ becomes a minimum at $r_2 \simeq 8$. The other dynamic parameter r_1 may also be regarded as adjustable. Then, the agreement between theory and experiment becomes better if a value somewhat smaller than unity is assigned to r_1. For convenience, however, we have fixed r_1 to unity

Table 8. Radii for Atactic Oligostyrene in Cyclohexane at 34.5 °C

	R_H, Å			
sample	from τ_Γ	from $[\eta]$	from D_t	$\langle S^2\rangle_z^{1/2}$, Å
OS3	3.7_5	4.8_3	4.3_5	
OS4	4.1_6	5.7_1	4.9_2	
OS5	4.4_7	6.3_1	5.0_4	4.7_5
OS6	5.0_0	6.8_1	5.5_1	5.1_4
OS8	6.0_3	7.7_6	6.8_1	5.8_9

as in our previous study of the dynamics of the HW chain. In Figure 11, we have omitted the theoretical values for $x_w \lesssim 10$, since the block-diagonal approximation[7] adopted in our theory breaks down in the range of such small N. It is seen that the theory may explain semiquantitatively the dependence of $k_BT\tau_\Gamma/\eta_0$ on x_w. If we assume, as in the previous study,[6] that the subbody is an oblate spheroid having the rotation axis of length a and the diameter d, then d is calculated to be equal to 10 Å from eqs 35–38 of ref 33 with the above values of a, r_1, and r_2. This value is rather in good agreement with the value 11 Å estimated previously[6] from the chemical structure of a-PS.

Further, it is pertinent to make here some remarks on the HW theoretical values themselves of $J_\Gamma(\Delta\omega)$. In the previous theoretical study,[8] we have examined the behavior of the eigenvalues $\lambda^j_{2,k}$ and the amplitudes A^j_k in eq 7 for the a-PS chain having the same model parameter values as those used above except for r_2, for which the value 10 instead of 8 has been adopted. The difference in the value of r_2 is small, and the previous results may also apply to the present case. It has been there shown that, among the five branches of eigenvalue spectra labeled with the superscript j (=−2 to 2), the branches except for $j = 0$ and −1 make negligibly small contributions to J_Γ and that the eigenvalues $\lambda^j_{2,k}$ with very small k in these two branches make actual contributions to J_Γ. Further, $\lambda^j_{2,k}$ are almost independent of k for very small k and the contribution of the $j = 0$ branch is much larger than that of the $j = -1$ one. Thus J_Γ may be well expressed in terms of a single Lorentzian, as mentioned in the preceding (Results) section. Although the relative contribution of the $j = -1$ branch increases with decreasing N, J_Γ may be still expressed in terms of a single Lorentzian, since its hwhm becomes close to that of the $j = 0$ branch, as shown in Figure 8 of ref 8. Therefore, the HW theory may explain well the spectra themselves obtained at finite concentrations as far as a-PS is concerned, although the theoretical results (for $r_2 = 8$) are not explicitly shown.

Next we consider the behavior of $k_BT\tau_\Gamma/\eta_0$ for $x_w \lesssim 10$, in which range our dynamic theory breaks down. As x_w is decreased, the orientations of the repeat units in an oligomer may be considered to change almost due to its entire rotation; i.e., the oligomer behaves nearly as a rigid body. Thus, we regard the "rigid" oligomer as a sphere having the hydrodynamic radius R_H, for simplicity, as done by Matsuo et al.[30] in their nuclear magnetic relaxation study. Further, if we assume that the oligomer as a whole has a cylindrically symmetric polarizability tensor, for simplicity, then its relaxation time τ_Γ, which is equal to $(6D_r)^{-1}$ with D_r the rotatory diffusion coefficient, may be given by

$$\tau_\Gamma = 4\pi\eta_0 R_H^3/3k_BT \qquad (17)$$

From this relation, the quantity $k_BT\tau_\Gamma/\eta_0$ is seen to just equal the volume of the sphere. The values of R_H calculated from eq 17 with the values of τ_Γ given in Table 2 for the samples OS3 through OS8 in cyclohexane at 34.5 °C are given in the second column of Table 8. In the table

are also given values of R_H calculated from intrinsic viscosities $[\eta]$ using the Einstein equation

$$[\eta] = 10\pi N_A R_H^3/3M \quad (18)$$

with N_A Avogadro's number, and from translational diffusion coefficients D_t using the Einstein–Stokes equation

$$D_t = k_B T/6\pi\eta_0 R_H \quad (19)$$

where we have used the values of $[\eta]$ and D_t determined previously[12,17] for the same samples under the same solvent condition. The three values of R_H for a given oligomer are seen to be rather in good agreement with each other.

These values are to be compared with those of the apparent root-mean-square radius of gyration $\langle S^2\rangle_s^{1/2}$ determined previously[15] from small-angle X-ray scattering measurements and given in the last column of Table 8. Recall that $\langle S^2\rangle_s$ is the coefficient of the squared scattering vector k^2 of the scattering function and may be regarded as the mean-square radius of gyration of the excess electron density. It is in general larger than the (usual) mean-square radius of gyration $\langle S^2\rangle$ of the chain contour and may be more suitable as the average dimension of the oligomer for the present problem. It is interesting to see that the values of $\langle S^2\rangle_s^{1/2}$ and R_H agree rather well with each other, indicating that the rigid sphere model is valid in this region in a first approximation.

The above results indicate that in such an oligomer region τ_Γ may be considered to be governed by the entire rotatory motion and may be related to the effective radius. In practice, we adopt $\langle S^2\rangle_s^{1/2}$ as such a radius since the HW theoretical expression as a *continuous* function of the total contour length L is available for $L \geq 0$ only for this quantity. Recall that the HW theories of $[\eta]$ and D_t are based on the touched-bead model, and therefore their theoretical values for the trimer through hexamer of a-PS cannot be calculated.[12,17] For the HW chain of total contour length L, $\langle S^2\rangle_s$ may be given by

$$\langle S^2\rangle_s = \langle S^2\rangle + S_c^2 \quad (20)$$

where $\langle S^2\rangle$ may be written in the form

$$\langle S^2\rangle = \lambda^{-2} f_S(\lambda L;\lambda^{-1}\kappa_0,\lambda^{-1}\tau_0) \quad (21)$$

and S_c is the (effective) radius of gyration of the cross section of the excess electron density distributed around the chain contour and has already been evaluated to be $\sqrt{11}$ Å for a-PS.[15] In eq 21, the function f_S is defined by

$$f_S(L;\kappa_0,\tau_0) = \frac{\tau_0^2}{\nu^2} f_{S,KP}(L) + \frac{\kappa_0^2}{\nu^2}\left[\frac{L}{3r}\cos\phi - \frac{1}{r^2}\cos(2\phi) + \frac{2}{r^3 L}\cos(3\phi) - \frac{2}{r^4 L^2}\cos(4\phi) + \frac{2}{r^4 L^2}e^{-2L}\cos(\nu L + 4\phi)\right] \quad (22)$$

with

$$\nu = (\kappa_0^2 + \tau_0^2)^{1/2} \quad (23)$$

$$r = (4 + \nu^2)^{1/2} \quad (24)$$

$$\phi = \cos^{-1}(2/r) \quad (25)$$

and with $f_{S,KP}$ being the function f_S for the Kratky–Porod wormlike chain[34] and given by

$$f_{S,KP}(L) = \frac{L}{6} - \frac{1}{4} + \frac{1}{4L} - \frac{1}{8L^2}(1 - e^{-2L}) \quad (26)$$

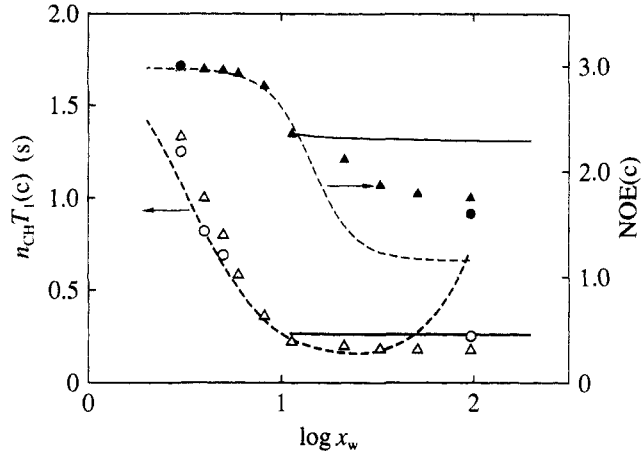

Figure 12. Plots of $n_{CH}T_1$(c) and NOE(c) of ^{13}C against the logarithm of x_w for the center methine carbon atoms (c) for a-PS in cyclohexane at 40 °C (with $n_{CH} = 1$): (○) T_1(c); (●) NOE(c). The solid and dashed curves represent the theoretical values for the HW model and the effective rigid sphere model, respectively. The unfilled and filled triangles represent the values of T_1 and NOE, respectively, calculated with $\tau_M = \tau_\Gamma^*$ (see the text).

Replacing R_H by $\langle S^2\rangle_s^{1/2}$ in eq 17, we have

$$\tau_\Gamma = 4\pi\eta_0\langle S^2\rangle_s^{3/2}/3k_B T \quad (27)$$

The values of τ_Γ calculated from eq 27 with eqs 20–26 are represented by the dashed curve in Figure 11. We note that the contour length L of the HW chain has been converted to x_w by the use of the relation $x_w = M_L L/M_0$. The dashed curve may reproduce satisfactorily the data points for $x_w \lesssim 10$, as expected.

From the above analysis, it may be concluded that the orientation of the polarizability tensor affixed to each repeat unit relaxes nearly due to the rotation of the entire chain for the oligomers with $x_w \lesssim 10$ but the former becomes completely independent of the latter for $x_w \gtrsim 10^2$.

Dependences of T_1 and NOE on x_w. Next we make an analysis of the present results for T_1 and NOE along the same line as in the last subsection. Figure 12 shows plots of T_1(c) and NOE(c) of ^{13}C for the center methine carbon atom (c) against the logarithm of x_w for a-PS in cyclohexane at 40 °C. The unfilled and filled circles represent the observed values of T_1 and NOE, respectively, and the solid curves represent the respective HW theoretical values calculated from eqs 11–15 with the same set of values of the static and dynamic model parameters as used in the last subsection. In the present case, we must specify the direction (α,β) of the C–H internuclear vector in the localized coordinate system, which is necessary for the calculation of the coefficients $A^j_{2,k}$ in eq 14. Thus the values 90° and 55° have been adopted as before[31] for the angles α and β in eq 26 of ref 31, respectively. (Note that, in the case of J_Γ, the values of the components of the polarizability tensor α have been specified.) For the Larmor angular frequencies ω_I and ω_S, we have used the values $2\pi \times 100.4 \times 10^6$ and $2\pi \times 399.2 \times 10^6$ rad/s, respectively, corresponding to our measurements. Further, we have adopted the values 1.09 Å of r and 0.690 cP of η_0 for cyclohexane at 40 °C. The calculation of the theoretical values has been limited again to the range of N $(=x_w) \gtrsim 10$. For such large N, the values of T_1 and NOE observed for the center (intermediate) methine carbon atoms are actually the mean values averaged over the position of ^{13}C, as noted above, so that we have presented the theoretical values averaged over p.

The HW theoretical values of both T_1 and NOE are almost independent of x_w (for $x_w \gtrsim 10$). Their asymptotic

values in the limit of $x_w \to \infty$ are 0.260 s and 2.29, respectively. The former is in good agreement with the value 0.25 s observed for the sample F1–2, while the latter is appreciably larger than the value 1.6 observed for the same sample. As was already reported,[6,31] our theory gives rather the poor prediction for the spin–spin relaxation time T_2 and NOE. It appears that the theoretical dependences of T_1 and NOE on x_w are inconsistent with the experimental results obtained by Matsuo et al.[30] for poly(fluorostyrene), which show that both T_1 and NOE increase appreciably with decreasing M_w for $10^3 \lesssim M_w \lesssim 10^4$. However, this disagreement may be regarded as arising from the use of different NMR spectrometers. (We note that they used a 60-MHz spectrometer.) The HW theoretical dependence of T_1 on x_w is again discussed later.

Now, as in the case of J_Γ, we consider the rigid sphere having the radius $\langle S^2 \rangle_s^{1/2}$, to which a C–H internuclear vector is affixed. T_1 and NOE may then be given by eqs 11 and 12 with J_m given by[35]

$$J_m(\omega) = \frac{2\tau_M}{1 + (\omega\tau_M)^2} \tag{28}$$

where τ_M is identical with τ_Γ given by eq 27. In Figure 12, the values of T_1 and NOE calculated from eqs 11 and 12, respectively, with eq 28 and with the above values of ω_I, ω_S, r, and η_0 are represented by the respective dashed curves. The dashed curve for T_1 is in good agreement with the data points for the samples OS3, OS4, and OS5 as in the case of τ_Γ.

The above agreement indicates that in the oligomer region the nuclear magnetic relaxation may be expressed in terms of the same τ_Γ as in the case of J_Γ. Then, since J_Γ may be expressed in terms of the single relaxation time τ_Γ even in the range of large x_w for which the polymer chain can be no longer represented by the rigid sphere, it may be expected that this is also the case with the nuclear magnetic relaxation, whose single relaxation time must be τ_Γ. Thus we calculate T_1 and NOE from eqs 11 and 12 with eq 28, where we equate τ_M to the scaled τ_Γ in cyclohexane at 40 °C, which we designate by τ_Γ^*, taking account of the differences in η_0 and T by the use of the relation

$$\tau_\Gamma^* = [(\eta_0/T)_{40}/(\eta_0/T)_{34.5}]\tau_\Gamma \tag{29}$$

with the observed values of τ_Γ in cyclohexane at 34.5 °C. The values of T_1 and NOE thus calculated for all samples are represented by the unfilled and filled triangles, respectively, in Figure 12. They agree well with the respective observed values. It may therefore be said that the above empirical treatment is approximately valid and that the two relaxation processes may give equivalent information about the local chain motions as far as a-PS is concerned.

It is seen from Figure 12 that the HW theoretical curve for T_1 agrees rather well with the values represented by the unfilled triangles in the range where the former is available. From the latter values, it may then be considered that, if the values of T_1 of ^{13}C were measured with a 400-MHz NMR spectrometer, they would be insensitive to the change in x_w for $10 \lesssim x_w \lesssim 100$ and be consistent with the HW theoretical values.

Correlation between τ_Γ and T_1. Finally, in this subsection, we examine the correlation between the two observables τ_Γ and T_1. Figure 13 shows double-logarithmic plots of $n_{CH}T_1(c)$ (in s) of ^{13}C of the center methine carbon atoms (c) against the scaled relaxation time τ_Γ^* (in s) for a-PS in cyclohexane at 40 °C. The solid curve represents

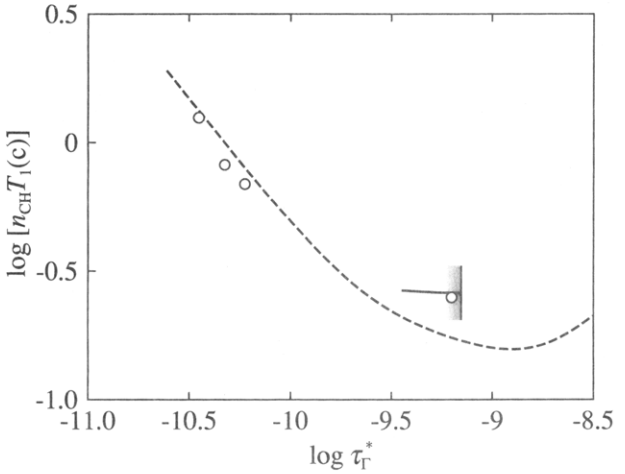

Figure 13. Double-logarithmic plots of $n_{CH}T_1(c)$ (in s) against τ_Γ^* (in s) for a-PS in cyclohexane at 40 °C (with $n_{CH} = 1$). The solid and dashed curves represent the theoretical values for the HW model and the effective rigid sphere model, respectively (see the text).

the HW theoretical values calculated in the same manner as above (in cyclohexane at 40 °C) for N (=x_w) ≥ 10. The right end point of the curve bounded by the vertical line segment with shade corresponds to the asymptotic value of τ_Γ^* in the limit of $x_w \to \infty$, and the other end point corresponds to $x_w = 10$. The dashed curve represents the values calculated for the rigid sphere model under the same solvent condition. In contrast to the case of the HW theory, τ_Γ, and hence τ_Γ^*, can increase infinitely with increasing x_w, so that the dashed curve does not have an end point in the limit of $x_w \to \infty$. The data points for the oligomer samples OS3, OS4, and OS5 follow the dashed curve, while that for the polymer sample F1-2 is close to the solid curve, as expected from the results shown in Figures 11 and 12.

We have already presented a similar plot in the previous theoretical study (see Figure 6 of ref 6), where the literature values of $n_{CH}T_1$ for various kinds of flexible polymers with sufficiently high M_w are plotted against the magnetic correlation times estimated for them on the basis of the HW theory. There, our major attention has been given to the dependence of T_1 on the kind of polymers, and it has been shown that the data points follow a single-composite curve irrespective of this kind. In the present case, x_w is varied as a parameter (hidden variable) for the single polymer species (a-PS). From the previous conclusion, the plot for a-PS in Figure 13 and those for other polymers may then be expected to make a single-composite curve. In order to confirm this, we need to make a similar study for other flexible polymers.

Conclusion

The power spectra $J_\Gamma(\Delta\omega)$ of the depolarized component of light scattered from a-PS in cyclohexane at 34.5 °C (Θ) and in CCl_4 at 25 °C have been found to be (single) Lorentzian independently of x_w for $3 \leq x_w \lesssim 100$. Then the relaxation time τ_Γ as defined as the reciprocal of the hwhm of J_Γ has been found to increase with increasing x_w and level off to an asymptotic value in the limit of $x_w \to \infty$ in each solvent. These results are consistent with our recent theoretical prediction on the basis of the HW chain model.[8] The values of the reduced quantity $k_B T\tau_\Gamma/\eta_0$ in the two solvents are in good agreement with each other for each sample, its asymptotic value in the limit of $x_w \to \infty$ being ca. 4×10^3 Å. A rather detailed analysis of the data

shows that the HW theory may explain rather satisfactorily the observed dependence of τ_Γ (or J_Γ) on x_w over that range of x_w for which the theory is applicable, i.e., for $x_w \gtrsim 10$, while the rigid sphere model having the radius equal to the apparent root-mean-square radius of gyration $\langle S^2 \rangle_s^{1/2}$ of the HW chain, newly introduced in this paper, may reproduce well the data for $x_w \lesssim 10$. This implies that the orientations of the repeat units relax nearly due to the rotation of the entire chain for the oligomers with $x_w \lesssim 10$, but the correlation between the local and global motions becomes weak with increasing x_w and completely vanishes for $x_w \gtrsim 100$.

As for the results of nuclear magnetic relaxation measurements, the HW theory can explain quantitatively those for T_1 but not for NOE for $x_w \gtrsim 10$. The failure in the explanation of NOE may be regarded as arising from some defects in our theory. On the other hand, the rigid sphere model may give a good explanation of both T_1 and NOE for $x_w \lesssim 10$ as in the case of τ_Γ. An analysis of the interrelation between the three observed quantities leads to the simple picture that the nuclear magnetic relaxation is also governed, although approximately, by a single relaxation time identical with τ_Γ.

It seems interesting and necessary to extend the present study to other flexible polymers and to examine the dependence of the above three dynamic properties on the static chain stiffness and local chain conformation. Thus we will do this for atactic oligo- and poly(methyl methacrylate)s in a forthcoming paper.

Acknowledgment. We have greatly benefited from valuable suggestions given by Professor T. Fujimoto of the Department of Engineering Science, Kyoto University, concerning the adoption of the ^{4}He hyperfine structure as a scale for the determination of the free spectral range of a Fabry–Perot interferometer. This research was supported in part by a Grant-in-Aid (04650809) from the Ministry of Education, Science, and Culture, Japan.

References and Notes

(1) Konishi, T.; Yoshizaki, T.; Shimada, J.; Yamakawa, H. *Macromolecules* **1989**, *22*, 1921 and succeeding papers.
(2) Yamakawa, H. *Annu. Rev. Phys. Chem.* **1984**, *35*, 23.
(3) Yamakawa, H. In *Molecular Conformation and Dynamics of Macromolecules in Condensed Systems*; Nagasawa, M., Ed.; Elsevier: Amsterdam, The Netherlands, 1988; p 21.
(4) Yamakawa, H. *Macromolecules* **1992**, *25*, 1912.
(5) Abe, F.; Einaga, Y.; Yoshizaki, T.; Yamakawa, H. *Macromolecules* **1993**, *26*, 1884 and succeeding papers.
(6) Yamakawa, H.; Yoshizaki, T.; Fujii, M. *J. Chem. Phys.* **1986**, *84*, 4693.
(7) Yamakawa, H.; Yoshizaki, T.; Shimada, J. *J. Chem. Phys.* **1983**, *78*, 560.
(8) Yoshizaki, T.; Yamakawa, H. *J. Chem. Phys.* **1993**, *99*, 9145.
(9) Ono, K.; Okano, K. *Jpn. J. Appl. Phys.* **1970**, *9*, 1356.
(10) Han, C. C.-C.; Yu, H. *J. Chem. Phys.* **1974**, *61*, 2650.
(11) Bauer, D. R.; Brauman, J. I.; Pecora, R. *Macromolecules* **1975**, *8*, 443.
(12) Einaga, Y.; Koyama, H.; Konishi, T.; Yamakawa, H. *Macromolecules* **1989**, *22*, 3419.
(13) Abe, F.; Einaga, Y.; Yamakawa, H. *Macromolecules* **1993**, *26*, 1891.
(14) Horita, K.; Abe, F.; Einaga, Y.; Yamakawa, H. *Macromolecules* **1993**, *26*, 5067.
(15) Konishi, T.; Yoshizaki, T.; Saito, T.; Einaga, Y.; Yamakawa, H. *Macromolecules* **1990**, *23*, 290.
(16) Abe, F.; Einaga, Y.; Yoshizaki, T.; Yamakawa, H. *Macromolecules* **1993**, *26*, 1884.
(17) Yamada, T.; Yoshizaki, T.; Yamakawa, H. *Macromolecules* **1992**, *25*, 377.
(18) Yamakawa, H.; Abe, F.; Einaga, Y. *Macromolecules* **1993**, *26*, 1898.
(19) Einaga, Y.; Abe, F.; Yamakawa, H. *Macromolecules* **1993**, *26*, 6243.
(20) Takaeda, Y.; Yoshizaki, T.; Yamakawa, H. *Macromolecules* **1993**, *26*, 3742.
(21) Yoshizaki, T.; Takaeda, Y.; Yamakawa, H. *Macromolecules* **1993**, *26*, 6891.
(22) Ouano, A. C.; Pecora, R. *Macromolecules* **1980**, *13*, 1167.
(23) Fred, M.; Tomkins, F. S.; Brody, J. K.; Hamermesh, M. *Phys. Rev.* **1951**, *82*, 406.
(24) See, for example: Hansen, J. P.; McDonald, I. R. *Theory of Simple Liquids*, 2nd ed.; Academic Press: New York, 1986; Chapter 8.
(25) Strehle, F.; Dorfmüller, Th.; Samios, D. *Macromolecules* **1992**, *25*, 3569.
(26) Ray, G. J.; Pauls, R. E.; Lewis, J. J.; Rogers, L. B. *Makromol. Chem.* **1985**, *186*, 1135.
(27) Konishi, T.; Yoshizaki, T.; Yamakawa, H. *Polym. J.* **1988**, *20*, 175.
(28) Sato, H.; Tanaka, Y.; Hatada, K. *Makromol. Chem., Rapid Commun.* **1982**, *3*, 181.
(29) Radiotis, T.; Brown, G. R.; Dais, P. *Macromolecules* **1993**, *26*, 1445.
(30) Matsuo, K.; Kuhlmann, K. F.; Yang, H. W.-H.; Gény, F.; Stockmayer, W. H.; Jones, A. A. *J. Polym. Sci., Polym. Phys. Ed.* **1977**, *15*, 1347.
(31) Yamakawa, H.; Fujii, M. *J. Chem. Phys.* **1984**, *81*, 997.
(32) Yamakawa, H.; Yoshizaki, T. *J. Chem. Phys.* **1981**, *75*, 1016.
(33) Yoshizaki, T.; Yamakawa, H. *J. Chem. Phys.* **1984**, *81*, 982.
(34) Kratky, O.; Porod, G. *Recl. Trav. Chim. Pays-Bas* **1949**, *68*, 1106.
(35) Solomon, I. *Phys. Rev.* **1955**, *99*, 559.